Evaluation of OLCI Neural Network Radiometric Water Products

Ilaria Cazzaniga, Giuseppe Zibordi, Frédéric Mélin, Ewa Kwiatkowska, Marco Talone, *Senior Member, IEEE*, David Dessailly, Juan I. Gossn, and Dagmar Müller

***Abstract*— Radiometric water products from the neural network (NNv2) in the alternative atmospheric correction (AAC) processing chain of Ocean and Land Colour Instrument (OLCI) data were assessed over different marine regions. These products, not included among the operational ones, were custom-produced from Copernicus Sentinel-3 OLCI Baseline Collection 3. The assessment benefitted of *in situ* reference data from the Ocean Color component of the Aerosol Robotic Network (AERONET-OC) from sites representative of different water types. These included clear waters in the Western Mediterranean Sea, optically complex waters characterized by varying concentrations of total suspended matter and chromophoric dissolved organic matter (CDOM) in the northern Adriatic Sea, and optically complex waters characterized by very high concentrations of CDOM in the Baltic Sea. The comparison of the water-leaving radiances $L_{WN}(\lambda)$ derived from OLCI data on board Sentinel-3A and Sentinel-3B with those from AERONET-OC confirmed consistency between the products from the two satellite sensors. However, the accuracy of satellite data products exhibited dependence on the water type. A general underestimate of $L_{WN}(\lambda)$ was observed for clear waters. Conversely, overestimates were observed for data products from optically complex waters with the worst results obtained for CDOM-dominated waters. These findings suggest caution in exploiting NNv2 radiometric products, especially for highly absorbing and clear waters.**

***Index Terms*— Ocean color, remote sensing, validation.**

I. Introduction

THE Ocean and Land Colour Instrument (OLCI, [1]) operates on board the Sentinel-3A (OLCI-A) and Sentinel-3B (OLCI-B) satellites since February 2016 and April 2018, respectively. The standard OLCI Level-2 ocean color products are generated through the baseline atmospheric correction (BAC [2]) processor originally conceived for waters exhibiting low optical complexity (i.e., Case-1 waters). Additionally, complementary data products are generated through the alternative atmospheric correction (AAC) processor to support ocean color applications in optically complex waters. In particular, AAC combines two distinct neural networks (NNs), one performing atmospheric correction to retrieve water reflectance $\rho_{WN}^{NN}(\lambda)$ and the other one quantifying the water inherent optical properties (IOPs) from $\rho_{WN}^{NN}(\lambda)$ [3]. These IOP data products are then used to determine the so-called OLCI NN operational products, i.e., the concentrations of total chlorophyll-a (CHL_NN) and total suspended matter (TSM_NN), and the total absorption coefficient of chromophoric dissolved organic matter (CDOM) and non-pigmented particles at the 443-nm center wavelength (ADG_443_NN). Even though $\rho_{WN}^{NN}(\lambda)$ is not included among the OLCI operational data products, it can be generated by any user through the Case-2 Regional CoastColour (C2RCC) processor [3] and ideally applied in combination with local bio-optical algorithms to generate regional data products. This potential application of $\rho_{WN}^{NN}(\lambda)$ data indicates the need for a thorough assessment to support their confident exploitation.

A new Baseline Collection 3 of Level-2 ocean color products (OL_L2M.003 [2]) has been recently released benefitting of System Vicarious Calibration (SVC) gains determined for both OLCI-A and OLCI-B. In this collection, the AAC products are generated through NNv2 neural network recently introduced with the objective to increase the accuracy of products from open ocean waters with respect to previous NNv1 [2] and to match NNv2 implemented in the C2RCC processor in the Sentinel Application Platform (SNAP).

A number of investigations already provided feedback on the accuracy of the NNv2 radiometric data products. Among these, Mograne *et al.* [4] compared the results from five atmospheric correction algorithms over optically complex waters in the Eastern English Channel and French Guiana. In that study, NNv2 exhibited better results than the other atmospheric correction algorithms, although affected by low accuracy at the blue spectral bands. Giannini *et al.* [5] documented large underestimates in the blue and also a saturation of remote sensing reflectance $R_{RS}(\lambda)$ for values above 0.008 sr^{-1} in the Northeast Pacific coastal waters. Finally, Vanhellemont and Ruddick [6] indicated general underestimates of radiometric products from NNv2 in the Belgian coastal turbid waters. Poor results were specifically reported at the 665- and 709-nm center wavelengths. It is important to mention, however, that the SVC gains were not applied to the NNv2 data products analyzed by [4] and [6]. Conversely, the SVC gains

Manuscript received October 12, 2021; accepted November 30, 2021. Date of publication December 17, 2021; date of current version January 12, 2022. This work was supported by the Joint Research Centre (JRC) through the Copernicus Ocean Long-term Observations for Remote Sensing applications project (COLORS). The support of the "Severo Ochoa Centre of Excellence" Accreditation (CEX2019-000928-S) is also acknowledged. *(Corresponding author: Ilaria Cazzaniga.)*

Ilaria Cazzaniga, Giuseppe Zibordi, and Frédéric Mélin are with the European Commission, Joint Research Centre (JRC), 21027 Ispra, Italy (e-mail: ilaria.cazzaniga@ec.europa.eu).

Ewa Kwiatkowska, David Dessailly, and Juan I. Gossn are with the EUMETSAT, Remote Sensing and Products Division, 64295 Darmstadt, Germany.

Marco Talone is with the Departament de Oceanografia Fisica, Institut de Ciències del Mar, 08003 Barcelona, Spain.

Dagmar Müller is with the Brockmann Consult GmbH, 21029 Hamburg, Germany.

Digital Object Identifier 10.1109/LGRS.2021.3136291

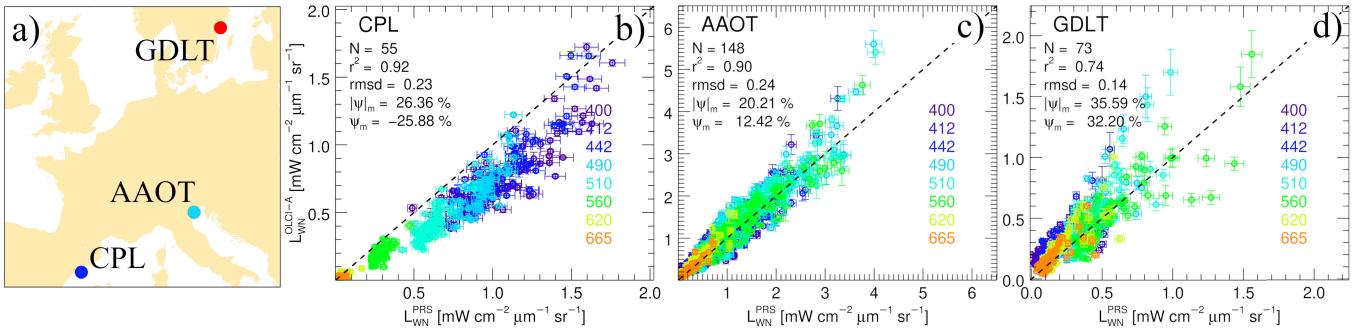

Fig. 1. (a) AERONET-OC sites location and (b)–(d) scatterplots of OLCI-A $L_{WN}^{NN}(\lambda)$ versus AERONET-OC $L_{WN}^{PRS}(\lambda)$ at the center wavelengths λ in the 400–665-nm spectral interval for different water types: (b) oligotrophic-mesotrophic (CPL); (c) optically complex (AAOT); (d) optically complex dominated by CDOM (GDLT). N indicates the number of matchups and r^2 is the determination coefficient across all points. The spectrally averaged root-mean-square difference (rmsd) is expressed in mW cm^{-2} μm^{-1} sr^{-1}. The spectrally averaged median relative difference (ψ_m) and absolute (unsigned) relative difference ($|\psi|_m$) are in %.

from OLCI operational processing Baseline 2 were applied to the data products examined by [5].

The objective of this work is to evaluate the accuracy of NNv2 radiometric data products across regions characterized by diverse water types. Specifically, by exploiting *in situ* reference data from the Ocean Color component of the Aerosol Robotic Network (AERONET-OC, [7]), the work presents an assessment of the NNv2 radiometric products from the OL_L2M.003 Collection for three European marine regions characterized by a gradient from oligotrophic–mesotrophic clear waters to various levels of concentrations of sediments and CDOM.

II. Data and Methods

A. In Situ Data

In situ normalized spectral water-leaving radiance $L_{WN}^{PRS}(\lambda)$ data corrected for the bidirectional effects [8] were considered from three European AERONET-OC sites [Fig. 1(a)]: 1) Casablanca Platform (CPL) in the Western Mediterranean Sea exhibiting occurrence of Case-1 waters (i.e., waters whose optical properties can often be described as a function of chlorophyll-a concentration); 2) Acqua Alta Oceanographic Tower (AAOT) in the northern Adriatic Sea for optically complex waters characterized by varying concentrations of sediments and CDOM; 3) Gustaf Dalen Lighthouse Tower (GDLT) in the Baltic Sea, also characterized by optically complex waters, but exhibiting high concentrations of CDOM. CPL data have been screened to only represent clear water cases by retaining exclusively those $L_{WN}^{PRS}(\lambda)$ spectra with the maxima at the blue center wavelengths (i.e., between 400 and 442 nm).

To minimize the corrections required to reduce the differences in spectral bands, the following analysis has been limited to the period 2018–2021. In fact, since 2018 measurements at a number of European AERONET-OC sites have been performed with CE-318T instruments with center wavelengths matching those of OLCI in the visible spectrum [9]. The AERONET-OC Level 2.0 data applied in the assessment were from the Version 3 database.

B. Satellite Data

OLCI Reduced Resolution (1.2 km) ocean color Level-2 products were custom-processed by EUMETSAT through Instrument Processing Facility (IPF) version 07.01 Collection 3 to ensure access to $\rho_{WN}^{NN}(\lambda)$ from the AAC processing chain. The NN devoted to the atmospheric correction in NNv2 was trained with radiative transfer simulations obtained with the successive order of scattering (SOS [10], [11]) code [3] using aerosol optical properties determined from AERONET [12] sun-photometric measurements performed at coastal sites. Lower boundary conditions have been imposed based on the same dataset of water reflectance applied to train the in-water component of NNv2 and determined with HydroLight simulations ([13], [14]).

The NN ingests the OLCI top of the atmosphere (TOA) reflectance corrected for gaseous absorption and for smile effects, with the SVC gains applied. In Collection 3, the SVC gains used in the AAC are the same as those obtained for BAC processing, i.e., not expressly derived for AAC: the impact on data products of such a solution has not yet been quantified. NN output is the directional water reflectance ρ_{WN}^{NN} from which the normalized water-leaving radiance $L_{WN}^{NN}(\lambda)$ is computed according to

$$L_{WN}^{NN}(\lambda) = \frac{\rho_{WN}^{NN}(\lambda) E_0(\lambda) C_{f/Q}(\lambda)}{\pi} \quad (1)$$

where $E_0(\lambda)$ is the mean spectral extra-atmospheric irradiance at mean earth–sun distance [15] and $C_{f/Q}(\lambda)$ is the correction for bidirectional effects consistent with that applied to the *in situ* data [8]. It is recognized that this latter correction was conceived for Case-1 waters and, consequently, the uncertainties resulting from its application to optically complex waters may be quite large.

C. Matchups Identification

Matchups (i.e., nearly simultaneous *in situ* and satellite data pairs) were created using the average $L_{WN}^{NN}(\lambda)$ of the 3 × 3 pixels centered at each AERONET-OC site. The matchups were included in the analysis whenever: 1) the time difference between the acquisition of *in situ* and satellite data was lower than 2 h; 2) none of the nine pixels was affected by any of the processing flags recommended for NN products (i.e., 'INVALID', 'LAND', 'COSMETIC', 'SUSPECT', 'CLOUD', 'CLOUD_AMBIGUOUS',

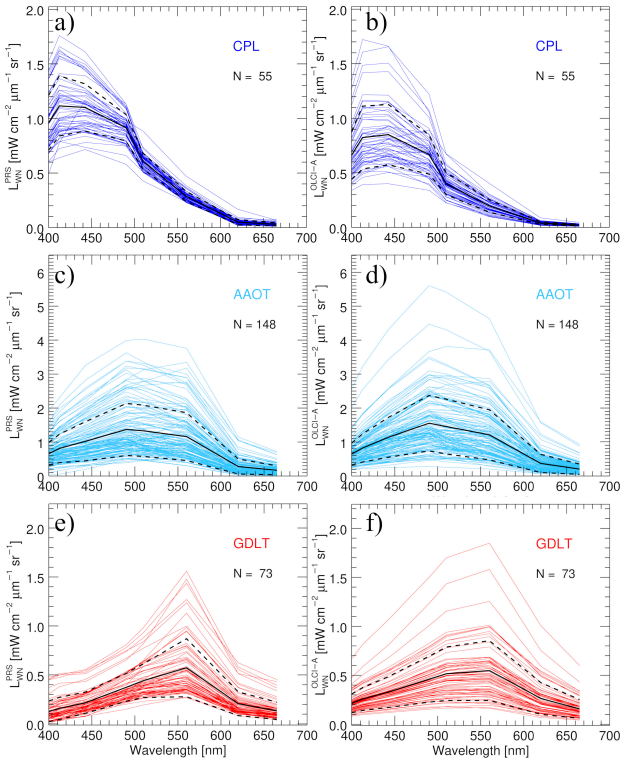

Fig. 2. (a), (c), and (e) AERONET-OC $L_{WN}^{PRS}(\lambda)$ and (b), (d), and (f) OLCI-A $L_{WN}^{NN}(\lambda)$ spectra for the matchup pairs representative of different water types: (a) and (b) oligotrophic-mesotrophic (CPL); (c) and (d) optically complex (AAOT); (e) and (f) optically complex dominated by CDOM (GDLT). N is the number of matchups. The continuous black lines indicate the median of the spectral values, while the dashed lines indicate ± 1 standard deviation.

'CLOUD_MARGIN', 'SNOW_ICE', 'HISOLZEN', 'SATURATED', 'HIGHGLINT', 'OCNN_FAIL') [2]; 3) the coefficient of variation (i.e., the ratio of standard deviation to mean) of $L_{WN}^{NN}(\lambda)$ at 560 nm for the set of nine pixels was lower than 20%; and 4) the satellite viewing zenith angle was lower than 60° and the sun zenith angle lower than 70°. For each site, the root-mean-square difference (rmsd), the median relative difference (ψ_m), and the median absolute (unsigned) relative difference ($|\psi|_m$) were determined from the available matchups. Data analysis was carried out for OLCI-A and OLCI-B separately.

III. Results

Figs. 1 and 2 display, for OLCI-A only, the satellite and *in situ* $L_{WN}(\lambda)$ scatterplots and the related spectra, respectively. Additionally, Fig. 3 summarizes the results from the statistical analysis of matchups at each center wavelength for both OLCI-A and OLCI-B. These results show an expected high consistency between radiometric data products from the two satellite sensors. However, the same results exhibit accuracies of satellite-derived versus AERONET-OC $L_{WN}(\lambda)$ largely varying across the three validation sites.

In clear waters at CPL, satellite-derived $L_{WN}^{NN}(\lambda)$ are largely underestimated with ψ_m varying between -22.0% at 560 nm and -15.0% at 412 nm for OLCI-A, and between -34.5% at 665 nm and -15.1% at 412 nm for OLCI-B. Values of r^2 ranging from 0.74 to 0.82 in the 400−442-nm spectral interval indicate a good correlation between satellite and *in situ* data. The correlation, on the other hand, rapidly degrades beyond 490 nm with r^2 close to zero in the red, where $L_{WN}^{PRS}(\lambda)$ values are very low and the related uncertainties are high. More in general, satellite-derived $L_{WN}^{NN}(\lambda)$ shows a flatter spectral shape in the green-red with respect to AERONET-OC $L_{WN}^{PRS}(\lambda)$ [see Fig. 2(a) and (b)]. In addition, the $L_{WN}^{NN}(\lambda)$ maximum usually appears at 442 nm rather than at 412 nm as for $L_{WN}^{PRS}(\lambda)$.

$L_{WN}^{NN}(\lambda)$ shows the best agreement with *in situ* data for the AAOT optically complex waters. Excluding the bands at 400 nm for OLCI-A and at 400 and 412 nm for OLCI-B, an overestimate is observed at the blue and green center wavelengths with ψ_m varying between $+0.8\%$ and $+14.1\%$. The dispersion of the compared data, as shown by $|\psi|_m$, decreases gradually from 400 to 560 nm and increases again in the red at 620 and 665 nm where it also shows larger overestimates. A high correlation between satellite and *in situ* data characterizes the comparison at all center wavelengths with minimum r^2 of 0.7 at 400 nm, increasing with wavelength. The median spectrum shown in Fig. 2(c) for OLCI-A (and similarly for OLCI-B) exhibits shape consistent with that of the *in situ* one [see Fig. 2(d)], except for a slightly steeper slope in the green.

The poorest results are obtained for the GDLT site representative of CDOM-dominated waters, with $|\psi|_m$ varying between 17.6% at 560 nm and 81.7% at 400 nm for OLCI-A, and 13.9% at 510 nm and 83.2% at 400 nm for OLCI-B. $L_{WN}^{NN}(\lambda)$ values in blue are generally largely overestimated while they exhibit a high dispersion in the red. Finally, although $L_{WN}^{NN}(\lambda)$ spectra exhibit maxima at 560 nm as $L_{WN}^{PRS}(\lambda)$, the overestimated values at 510 nm appreciably affect the shape of satellite-derived spectra [see Fig. 2(e) and (f)].

IV. Discussion

A new water bio-optical model was implemented in NNv2 to better accommodate the large variability of natural waters with respect to NNv1. To do so, the number of training samples of water reflectance was increased implying an extension of the ranges of the water IOPs. Still, large overestimates and inconsistent spectral shapes affect $L_{WN}^{NN}(\lambda)$ particularly for the highly absorbing waters at GDLT. This inconsistency of the spectral shape was already documented for the NNv1 products in the Baltic Sea by Kyryliuk and Kratzer [16], who also reported a shift in $R_{RS}(\lambda)$ peak from 560 to 490 nm in near-coastal areas explained by a poorer performance of the atmospheric correction in the blue spectral region.

Inaccurate determinations of $L_{WN}^{NN}(\lambda)$ for those waters could be likely due to a lack of representativeness in the dataset of the reflectance spectra applied to define boundary conditions in the training of the NNv2 component supporting the atmospheric correction. Indeed, this dataset is only a part of the full set of simulations generated with HydroLight. IOP and reflectance values for some spectral bands have been in fact limited to the natural range and the covariance of the open ocean and coastal measurements included in the MEris MAtchup In-situ Database (MERMAID), the NASA bio-Optical Marine Algorithm Dataset (NOMAD, [17]) and the CoastColour database [18].

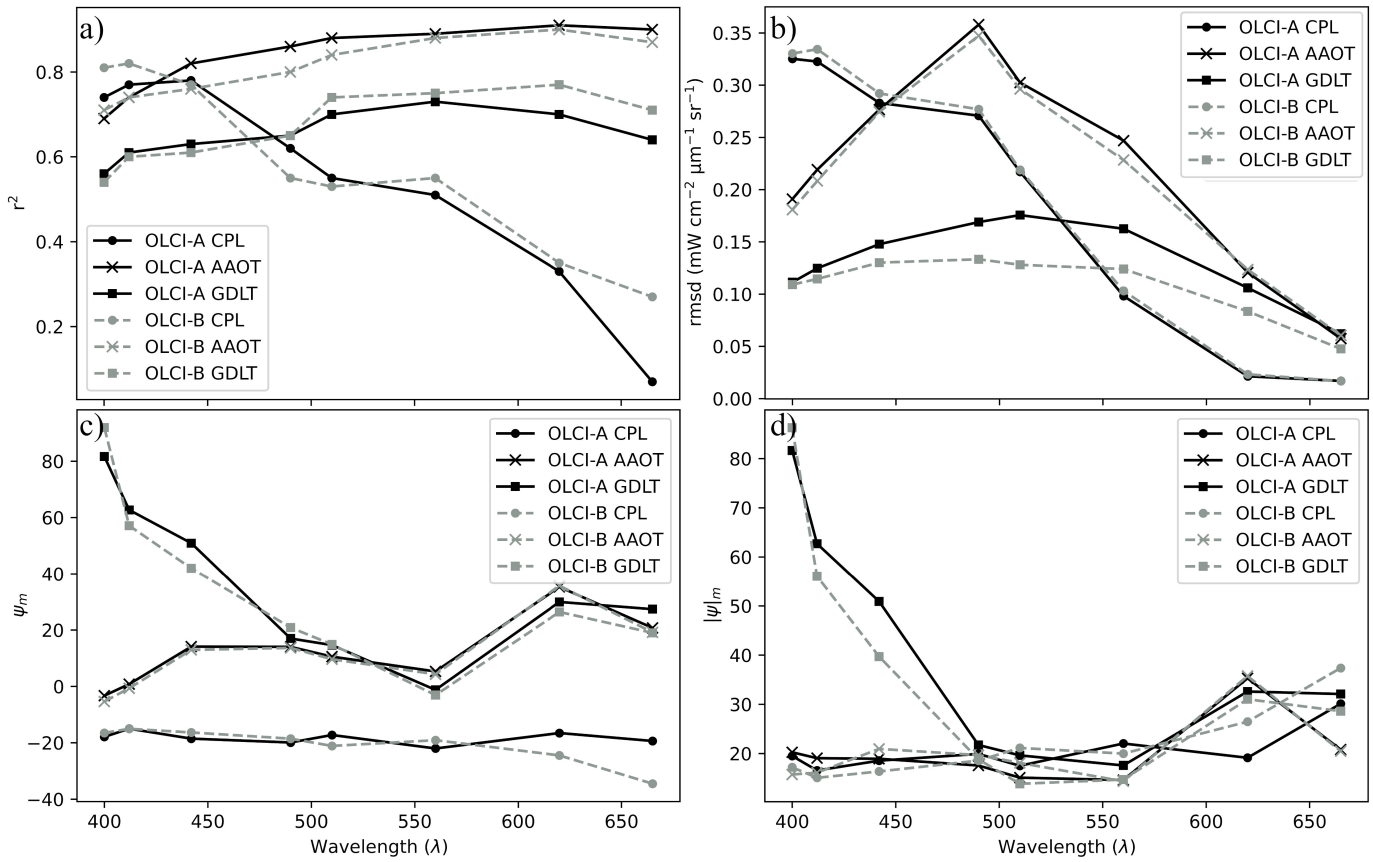

Fig. 3. Results from the comparison of OLCI-A and OLCI-B $L_{\mathrm{WN}}^{\mathrm{NN}}(\lambda)$ with AERONET-OC $L_{\mathrm{WN}}^{\mathrm{PRS}}(\lambda)$ at the three selected sites: (a) determination coefficients (r^2), (b) root-mean-square difference (rmsd), (c) median relative difference (ψ_{m}), and (d) absolute (unsigned) relative difference ($|\psi|_{\mathrm{m}}$) (these latter are expressed in %). The number of matchups for OLCI-A is 55, 148, and 73 and for OLCI-B is 64, 133, and 77, at CPL, AOT, and GDLT, respectively.

The comparison of the results from $L_{\mathrm{WN}}^{\mathrm{NN}}(\lambda)$ assessment with those obtained for BAC products in former investigations for equivalent water types [19] indicates that accuracies of NNv2 radiometric products are more dependent on water type and wavelength. For example, over the CPL blue waters, $L_{\mathrm{WN}}^{\mathrm{NN}}(\lambda)$ shows a consistent underestimate of approximately 20%, while BAC products are much closer to *in situ* data and show ψ_{m} values varying between -2% and $+6\%$ at the blue center wavelengths up to 510 nm, and then underestimates of 4%–6% at 560 nm, largely increasing in the red spectral region. Over CPL, $L_{\mathrm{WN}}^{\mathrm{NN}}(\lambda)$ exhibits a higher correlation with $L_{\mathrm{WN}}^{\mathrm{PRS}}(\lambda)$ at the blue center wavelengths when compared with BAC products, but at 560 nm the correlation is lower and comparable to that characterizing the other center wavelengths. Over generic optically complex waters such as those characterizing the AAOT site, NNv2 outperforms BAC only at the shorter blue bands below 442 nm, where BAC shows $|\psi|_{\mathrm{m}}$ values up to 43.5%. Otherwise, NNv2 performance appears degraded with respect to BAC. Over CDOM-dominated optically complex waters, $L_{\mathrm{WN}}^{\mathrm{NN}}(\lambda)$ products show overestimates, whereas BAC products show underestimates. For these water types, the correlation with *in situ* data at wavelengths below 560 nm is higher for NNv2 with respect to BAC products (these latter show values varying between 0.00 and 0.58 between 400- and 510-nm center wavelengths). It is, however, acknowledged that for CDOM-dominated and generic complex waters, additional sites besides GDLT and AAOT were considered in [19].

V. Conclusion

OLCI NNv2 $L_{\mathrm{WN}}^{\mathrm{NN}}(\lambda)$ products in the 400–665-nm spectral region have been assessed using *in situ* AERONET-OC data representing different water types. The analysis has shown comparable results for OLCI-A and OLCI-B and a strong dependence of products accuracy on water type. A general underestimate is shown for the CPL clear waters. Conversely, overestimates (with ψ_{m} ranging between $+0.8\%$ and $+35.7\%$) characterize the optically complex waters at AAOT at almost all center wavelengths. Finally, much poorer is the result from the assessment for the CDOM-dominated waters at GDLT, where $L_{\mathrm{WN}}^{\mathrm{NN}}(\lambda)$ values are widely overestimated (in the blue up to $+81.7\%$ for OLCI-A and $+92.0\%$ for OLCI-B, according to ψ_{m}).

These results indicate that NNv2 exhibits better performance in optically complex waters, such as those characterizing the northern Adriatic Sea at the shorter blue center wavelengths below 442 nm, where it outclasses BAC. However, these same results suggest caution in exploiting NN radiometric products in regions characterized by oligotrophic–mesotrophic or highly absorbing waters.

Finally, overall results confirm the importance of a globally distributed dataset of *in situ* measurements, both for training the NNs and validating the output from the processing algorithms.

ACKNOWLEDGMENT

The authors would like to thank the AERONET Team for processing and distributing the data from the Ocean Color component of the Aerosol Robotic Network.

REFERENCES

[1] C. Donlon *et al.*, "The global monitoring for environment and security (GMES) Sentinel-3 mission," *Remote Sens. Environ.*, vol. 120, pp. 37–57, May 2012, doi: 10.1016/j.rse.2011.07.024.

[2] EUMETSAT. (2021). *Sentinel-3 OLCI L2 Report for Baseline Collection OL_L2M_003—EUM/RSP/REP/21/1211386*. [Online]. Available: https://www.eumetsat.int/media/47794

[3] C. Brockmann, R. Doerffer, M. Peters, K. Stelzer, S. Embacher, and A. Ruescas, "Evolution of the C2RCC neural network for Sentinel 2 and 3 for the retrieval of ocean colour products in normal and extreme optically complex waters," in *Proc. Living Planet Symp.*, vol. 740, L. Ouwehand, Ed., Prague, Czech Republic, May 2016, p. 54.

[4] M. A. Mograne, C. Jamet, H. Loisel, V. Vantrepotte, X. Mériaux, and A. Cauvin, "Evaluation of five atmospheric correction algorithms over French optically-complex waters for the Sentinel-3A OLCI ocean color sensor," *Remote Sens.*, vol. 11, no. 6, pp. 668–693, 2019, doi: 10.3390/rs11060668.

[5] F. Giannini, B. P. V. Hunt, D. Jacoby, and M. Costa, "Performance of OLCI Sentinel-3A satellite in the Northeast Pacific coastal waters," *Remote Sens. Environ.*, vol. 256, Apr. 2021, Art. no. 112317, doi: 10.1016/j.rse.2021.112317.

[6] Q. Vanhellemont and K. Ruddick, "Atmospheric correction of Sentinel-3/OLCI data for mapping of suspended particulate matter and chlorophyll-a concentration in Belgian turbid coastal waters," *Remote Sens. Environ.*, vol. 256, Apr. 2021, Art. no. 112284, doi: 10.1016/j.rse.2021.112284.

[7] G. Zibordi *et al.*, "AERONET-OC: A network for the validation of ocean color primary products," *J. Atmos. Ocean. Technol.*, vol. 26, no. 8, pp. 1634–1651, Aug. 2009, doi: 10.1175/2009JTECHO654.1.

[8] A. Morel, D. Antoine, and B. Gentili, "Bidirectional reflectance of oceanic waters: Accounting for Raman emission and varying particle scattering phase function," *Appl. Opt.*, vol. 41, no. 30, pp. 6289–6306, 2002, doi: 10.1364/AO.41.006289.

[9] G. Zibordi *et al.*, "Advances in the ocean color component of the aerosol robotic network (AERONET-OC)," *J. Atmos. Ocean. Technol.*, vol. 38, no. 4, pp. 725–746, Apr. 2021, doi: 10.1175/jtech-d-20-0085.1.

[10] J. Lenoble, M. Herman, J. L. Deuzé, B. Lafrance, R. Santer, and D. Tanré, "A successive order of scattering code for solving the vector equation of transfer in the earth's atmosphere with aerosols," *J. Quant. Spectrosc. Radiat. Transf.*, vol. 107, no. 3, pp. 479–507, Oct. 2007, doi: 10.1016/j.jqsrt.2007.03.010.

[11] M. Chami, R. Santer, and E. Dilligeard, "Radiative transfer model for the computation of radiance and polarization in an ocean–atmosphere system: Polarization properties of suspended matter for remote sensing," *Appl. Opt.*, vol. 40, no. 15, pp. 2398–2416, May 2001, doi: 10.1364/AO.40.002398.

[12] B. N. Holben *et al.*, "AERONET—A federated instrument network and data archive for aerosol characterization," *Remote Sens. Environ.*, vol. 66, no. 1, pp. 1–16, 1998, doi: 10.1016/S0034-4257(98)00031-5.

[13] C. Mobley, *Light and Water: Radiative Transfer in Natural Waters*. New York, NY, USA: Academic, 1994.

[14] C. D. Mobley, "A numerical model for the computation of radiance distributions in natural waters with wind-roughened surfaces," *Limnol. Oceanogr.*, vol. 34, no. 8, pp. 1473–1483, Dec. 1989, doi: 10.4319/lo.1989.34.8.1473.

[15] G. Thuillier *et al.*, "The solar spectral irradiance from 200 to 2400 nm as measured by the SOLSPEC spectrometer from the ATLAS and EURECA missions," *Sol. Phys.*, vol. 214, no. 1, pp. 1–22, May 2003, doi: 10.1023/A:1024048429145.

[16] D. Kyryliuk and S. Kratzer, "Evaluation of Sentinel-3A OLCI products derived using the Case-2 Regional CoastColour processor over the Baltic sea," *Sensors*, vol. 19, no. 16, p. 3609, Aug. 2019, doi: 10.3390/s19163609.

[17] P. J. Werdell and S. W. Bailey, "An improved *in-situ* bio-optical data set for ocean color algorithm development and satellite data product validation," *Remote Sens. Environ.*, vol. 98, no. 1, pp. 122–140, Sep. 2005, doi: 10.1016/j.rse.2005.07.001.

[18] B. Nechad *et al.*, "CoastColour Round Robin data sets: A database to evaluate the performance of algorithms for the retrieval of water quality parameters in coastal waters," *Earth Syst. Sci. Data*, vol. 7, no. 2, pp. 319–348, Nov. 2015, doi: 10.5194/essd-7-319-2015.

[19] G. Zibordi *et al.*, "Assessment of OLCI-A and OLCI-B radiometric data products," *Remote Sens. Environ.*, to be published.